Journal of Materials Chemistry B

ROYAL SOCIETY OF CHEMISTRY

PAPER

View Article Online
View Journal | View Issue

Cite this: J. Mater. Chem. B, 2025, 13, 2114

Development of 3D-printed conducting microneedle-based electrochemical point-of-care device for transdermal sensing of chlorpromazine†

Sachin Kadian,[a] Siba Sundar Sahoo,[b] Shubhangi Shukla[a] and Roger J. Narayan *[ab]

Despite the various benefits of chlorpromazine, its misuse and overdose may lead to severe side effects, therefore, creating a user-friendly point-of-care device for monitoring the levels of chlorpromazine drug to manage the potential side effects and ensure the effective and safe use of the medication is highly desired. In this report, we have demonstrated a simple and scalable manufacturing process for the development of a 3D-printed conducting microneedle array-based electrochemical point-of-care device for the minimally invasive sensing of chlorpromazine. We used an inkjet printer to print the carbon and silver ink onto a customized 3D-printed ultrasharp microneedle array for the preparation of counter, working, and reference electrodes. After physical characterization and electrochemical parameter optimization, the developed microneedle array-based three-electrode system was explored for the detection of chlorpromazine. The analytical results showed high sensitivity and selectivity toward chlorpromazine with a good linearity range from 5–120 μM and a low detection limit (0.09 μM). The proof-of-concept study results obtained from the skin-mimicking model indicated that the developed conductive microneedle array-based sensor can easily monitor the micromolar levels of chlorpromazine in artificial interstitial fluid; this type of system can be further explored for the development of other minimally invasive electrochemical biosensors.

Received 12th August 2024,
Accepted 24th December 2024

DOI: 10.1039/d4tb01808g

rsc.li/materials-b

1. Introduction

Antipsychotics or neuroleptics are drugs that are generally used to manage the symptoms of psychiatric disorders such as schizophrenia, bipolar disorder, and severe agitation.[1,2] Chlorpromazine hydrochloride is the most commonly used first-generation antipsychotic drug to treat the disorders mentioned above by blocking the neurotransmitter involved in regulating mood, behavior, and perception, reducing its activity.[3,4] It is recommended as a shock-reducing and sedative drug after surgical procedures and is also utilized to treat tetanus, nausea, and critical hiccups. Due to the beneficial anti-serotonergic and antihistaminergic properties of chlorpromazine hydrochloride, the World Health Organization (WHO) describes this typical neuroleptic drug as an important medicine.[5,6] Regardless of its various biomedical significance, the use of chlorpromazine hydrochloride may lead to severe side effects, including tardive dyskinesia, orthostatic hypotension, decreased white blood cell count, Parkinsonism, hyperprolactinemia, dropping of the seizure threshold, blurred vision, urinary retention, cognitive impairment, and neuroleptic malignant syndrome.[7–9] Therefore, the Food and Drug Administration (FDA) limited the intake level of chlorpromazine to 0.125 mM and 0.235 mM for children below 5 years old and 6–12 years old, respectively.[10] Thus, it is important for individuals taking chlorpromazine or any other antipsychotic medication to monitor the levels of the drug for management of the potential side effects in order to facilitate the effective and safe use of the medication.

Considering the importance of the problem, various analytical techniques, including spectrophotometry, high-performance liquid chromatography, mass spectrometry, and chemiluminescence, have been used to determine the concentration of chlorpromazine in blood samples.[6,7,11–14] Although these analytical techniques are sufficiently sensitive for the determination of chlorpromazine levels, these methods require the use of costly equipment, environmentally unfriendly chemicals, complex sample pretreatment steps, prolonged extraction and analysis

[a] Joint Department of Biomedical Engineering, University of North Carolina and North Carolina State University, Raleigh, NC 27695, USA. E-mail: rjnaraya@ncsu.edu, skadian@ncsu.edu
[b] Department of Materials Science and Engineering, North Carolina State University, Raleigh, NC 27695, USA

† Electronic supplementary information (ESI) available. See DOI: https://doi.org/10.1039/d4tb01808g

processes, trained technicians, and the production of large amounts of liquid waste, which limit their feasibility for onsite and rapid monitoring applications. Because of their good sensitivity, low detection limit, high specificity, rapid analysis, simple operation procedures, portability, and ease of fabrication, the low-cost electrochemical sensing platforms for onsite detection of several types of drugs, opioids, and biomolecules have garnered substantial attention from both academia and the pharmaceutical industry.[15–23] For instance, Wang *et al.* developed an antimony vanadate ($SbVO_4$) microsphere-modified glassy carbon electrode-based electrochemical sensing approach for the amperometric evaluation of chlorpromazine hydrochloride in blood serum samples, which provided a lower limit of detection of 0.11 nM.[10] Lu *et al.* introduced a new molecularly imprinted polymer-based Ni-MOF/Fe-MOF-5 hybrid gold nanoparticles modified glassy carbon electrode with a signal on–off ratiometric electrochemical sensing approach for chlorpromazine detection, which provided a detection limit of 0.025 μM.[24] Liu *et al.* used vertically ordered mesoporous silica films and electrochemically reduced graphene oxide nanosheets modified screen-printed carbon electrodes for the development of an electrochemical sensing platform for the detection of chlorpromazine in blood samples, which provided a 16 nM detection limit.[25] Palakollu *et al.* prepared a glassy carbon electrode that was decorated with a nitrogen-doped carbon dots/cuprous oxide composite for electrochemical sensing of chlorpromazine in human urine, which provided the detection limit of 25 nM.[26] Although there are previous reports on electrochemical sensing platforms for chlorpromazine detection, these sensing probes rely on the collection of a blood sample, laboratory instrumentation, unwanted pain during blood acquisition from finger pricking, and modification of the electrode surface; they are unable to monitor the chlorpromazine levels in a rapid, simple and straightforward way at the point-of-care site. Thus, the fabrication of a portable, minimally invasive, and point-of-care sensing approach that can address the aforementioned issues by onsite detection of chlorpromazine levels in interstitial fluid with enhanced analytical performance is highly desirable.

Recently, the advantages of wearable and portable sensing technologies have garnered interest from scientists for the fabrication of customized and straightforward-to-use healthcare devices.[27–31] Among several wearable sensing methods proposed in the last few years, microneedle-based sensing platforms have attracted significant attention for the rapid, simple, and minimally invasive monitoring of different biomarkers present in interstitial fluid.[32–36] Due to the micron size and minimally invasive characteristics of the microneedle array, microneedles can smoothly puncture the stratum corneum layer found in human skin and create artificial pores for biomarker monitoring, with minimal discomfort and tissue inflammation.[37–40] These micrometer-size wearable electrochemical sensing platforms depend on the surface of the microneedle array encompassing the biosensing electrodes at their tips and offer simultaneous monitoring of multiple biomarkers that are present in the interstitial fluid.[41,42] Due to their several advantages, microneedle array-based sensing approaches have been described for the detection of different analytes, including lidocaine, glucose, ketones, dopamine, cholesterol, potassium ions, alcohol, L-dopa, and lactate.[28,41,43–47] However, to the best of our knowledge, no efforts have been made involving the fabrication of nonmetallic 3D-printed conducting microneedle-based sensors to detect chlorpromazine in interstitial fluid.

Therefore, the present work demonstrates the development of a 3D-printed conducting microneedle array-based electrochemical point-of-care device for the detection of chlorpromazine. The developed microneedle-based sensing platform utilizes microneedle technology, 3D printing, and inkjet printing for the fabrication of conducting microneedle array-based three-electrode electrochemical systems. The fabricated sensing platform utilized an inkjet printer to print the carbon and silver ink onto a customized 3D-printed ultrasharp microneedle array for the preparation of counter, working, and reference electrodes. To achieve highly sensitive detection of the analyte, the working electrode microneedle array was further modified with freshly prepared carbon dots. Before sensing chlorpromazine, the electrochemical, analytical, structural, and morphological characteristics of the as-prepared microneedle-based sensing platform were investigated. Under the optimized parameters, the developed wearable microneedle-based point-of-care device demonstrated appropriate sensitivity and selectivity towards chlorpromazine. The practicability and real-time sensing potential of the wearable microneedle-based sensor were further examined by investigating the analytical performance of the device *via* a skin-mimicking parafilm layer in the artificial interstitial fluid. The collected results indicated that through the use of inkjet printing and 3D printing techniques, a simple, economical, user-friendly, and minimally invasive wearable microneedle-based electrochemical point-of-care device could be fabricated for wireless detection of chlorpromazine. Moreover, the customized fabrication of a novel 3D-printed microneedle-based wearable sensor demonstrated here can also be explored for the development of other wearable biosensors.

2. Experimental section

2.1 Materials and methods

All commercial-grade conductive inks, plastics, paper, glass, and metal substrates were purchased from NovaCentrix, USA. Interference compounds, analytes, and other chemicals, including potassium ferricyanide, chlorpromazine, citric acid, urea, ascorbic acid, caffeine, uric acid, phosphate buffer, dopamine, and acetaminophen were obtained from Sigma Aldrich, USA. Milli Q system was used to obtain the fresh deionized water (18.2 MΩ cm at 25 °C) for the preparation of all dilutions and solutions. All other reagents were of analytical grade; these reagents were used without any modifications.

2.2 Synthesis of carbon dots

Carbon dots were synthesized using previously reported bottom-up methodology *via* direct pyrolysis of citric acid and urea.[46,48,49] In this approach, 1.8 g citric acid and 0.5 g urea powder were crushed in a ceramic mortar and kept at 220 °C for

12 min in a glass beaker. After 12 minutes, the white-colored powder turned into an orange-colored liquid, which was added to freshly prepared 25 mL (10 mg mL^{-1}) NaOH solution with vigorous stirring. After the neutralization of pH, the resultant solution having carbon dots was filtered through a 0.22 μm pore size syringe filter to eliminate the unreacted large particles and remaining reagents, followed by further dialysis filtration. The filtered and purified solution was kept in a refrigerator at 4 °C until further use.

2.3 Microneedle design and fabrication

A high-resolution and ultra-sharp microneedle array structure having 67 conical shape needles (30, 25, and 12 needles for counter, working and reference electrode, respectively) with height of 1200 μm and base diameter of 350 μm was designed using SolidWorks 2016 software provided by Dassault Systems and printed using a Boston Micro Fabrication (BMF) S130 3D-printer (working on Projection Micro Stereolithography (PμSL) technology). For 3D printing of the microneedle array, the SolidWorks design file was sliced into layers *via* BMF Slicer software to generate a 3D printing instrument that was compatible with writing language code. A yellow biocompatible photoreactive BIO resin obtained from BMF was used for the microneedle array fabrication. The biological properties of the BIO resin were previously evaluated by the manufacturer *via* the ISO 10 993-12: 2012 *in vitro* cytotoxicity test; the ISO 10 993-10: 2010, ISO 10 993-12: 2012, and ISO10 993-2: 2006 skin irritation test; and the ISO 10 993-12: 2012 acute systemic toxicity test. The Young's modulus and hardness value of the resin were previously calculated using a Ubi-1 nanoindenter (Hysitron, microneedle, USA) having Berkovich-type tip and found to be 3.29 ± 0.12 GPa and 302.19 ± 10.44 MPa (mean value ± standard deviation value), respectively.[19] Upon the printing step was completed, the 3D-printed parts were rinsed in isopropyl alcohol to remove the unpolymerized resin and further kept at 45 °C under a 405 nm wavelength lamp (Formlabs Inc., USA) for 10 minutes. To make the 3D-printed microneedle array a three-electrode system, commercially available carbon and silver inks were inkjet-printed using a Fujifilm Dimatix DMP-2831 material printer and DMCLCP-11610 inkjet cartridges. To complete this step, the 3D-printed microneedle array was placed onto the printer platen, and a customized design was loaded into an inkjet printer-integrated computer system. To avoid physical contact with the printing jet and retain consistency in terms of the distance of droplet flight, the substrate thickness was set to 3500 μm. Two separate inkjet cartridges were loaded with 1.5 mL of each ink and deposited one by one. Afterward, the conductive ink-deposited microneedle array was kept at 100 °C in a conventional oven for 15 minutes for further curing process of the ink. To make good electrical connections, a conductive silver epoxy was lined over the connecting legs and further cured at 80 °C for 25 min. To construct a micro-nano hierarchical structure on the microneedle surface, as prepared carbon dots were drop cast onto the working electrode (array of 25 microneedles), followed by the deposition of a protective Nafion layer to avoid possible leaching from the needle surface. To fully assemble the device, a 3D printed very thin cover (0.25 mm thick) was incorporated to shield the electronic pathways and avoid any unwanted electrical contacts other than at the tip area.

2.4 Physical and electrochemical characterization

A Hitachi SU3900 variable pressure scanning electron microscope (VPSEM, Tokyo, Japan) equipped with solid state backscattered electron detector, which delivers an accelerating voltage between 0.3 to 30 kV, was used for the topological and morphological evaluation of the 3D-printed microneedle array before and after the deposition of conductive ink. A battery-powered rechargeable and hand-held PalmSens4 potentiostat (PalmSens BV) was used for electrochemical analysis, including electrode stability, analyte detection, temporal stability, and interference studies of the as-developed conductive microneedle array. All electrochemical investigations were performed wirelessly at room temperature, and the acquired dataset was also transferred wirelessly for further analysis.

2.5 Skin penetration test

The skin penetration capability of the as-developed microneedle-based transdermal sensing platform was investigated *ex vivo* on porcine skin. To complete this step, the recently slaughtered pig skin was obtained from a regional provider and cleaned with sanitizing wipes. Next, the sanitized skin patch was fixed on a glass Petri plate and subjected to puncture with the as-developed microneedle array. Further, to demonstrate the microneedle array generated pores on the pig skin patch, an optical microscope was used to capture the images of the pig skin surface before and after skin penetration by the microneedle array.

2.6 Electrochemical sensing of chlorpromazine

Before using the as-developed microneedle-based sensing platform for chlorpromazine sensing, the electrochemical characteristics and stability of the conductive microneedle-based working electrode were studied at a constant scan rate of 50 mV s^{-1} in a ferricyanide solution (3 mM) through the cyclic voltammetry technique. Next, the change in the electroanalytical performance of the carbon dots-modified microneedle-based working electrode was also examined under the same experimental settings. Afterward, the chlorpromazine sensing potential of the microneedle-based sensing platform was studied by gathering the differential pulse voltammetry spectra (between a potential window ranging from −0.2 to 0.5 V with a pulse time of 0.02 s and potential step of 0.01 V) in fresh buffer electrolyte solution after adding various concentrations of chlorpromazine that were prepared from the fresh stock solution (1.0 mg mL^{-1}). Next, the long-term storage stability of the developed microneedle sensor was evaluated by assessing the variation in the analytical characteristics of the sensor for three weeks.

2.7 Proof-of-concept study

To understand the real-time application potential of the fully assembled microneedle-based sensor, the electrochemical

sensing efficacy of the carbon dots decorated conductive microneedle-based working electrode was investigated in artificial interstitial fluid by collecting the differential pulse voltammetry response *via* a skin-mimicking parafilm layer and phantom del model. In this approach, a Petri dish containing artificial interstitial fluid was spiked with different chlorpromazine concentrations and carefully covered with parafilm tape. Next, the fully assembled microneedle-based sensor was smoothly pressed against the parafilm tape in such a manner that the tips of microneedles could easily penetrate the skin-mimicking layer and interact with the underneath analyte solution. Afterward, the differential pulse voltammetry response was recorded for a varying concentration of chlorpromazine between a potential window ranging from −0.1 to 0.5 V and a potential step of 0.01 V. Further, a skin-mimicking phantom gel was made utilizing the previously reported process[28,33] and the as-prepared microneedles-based sensing platform was examined in the chlorpromazine infused phantom gel after 2 minutes of gel and needle tips contact.

3. Results and discussion

3.1 Design and working of the microneedle-based sensing platform

The minimally invasive detection of biomarkers using conducting microneedles has demonstrated great potential for the development of next-generation wearable devices. Previous efforts to prepare a working electrode on the tip of a microneedle have involved metallic microneedles, which are associated with expensive and complex manufacturing procedures; these limitations could make it difficult to reach the full potential of microneedle technology.[50] We utilized additive manufacturing approaches, including 3D printing and inkjet printing, for the fabrication of tailored and scalable polymeric microneedle arrays. Fig. 1 shows a schematic diagram of the stepwise fabrication process that was used to prepare the microneedle array-based sensing platform. The customized computer-aided design of the microneedle array was 3D printed using a BMF 3D printer and subjected to an inkjet printing process to make the needles and contact pads conductive. Next, to make a three-electrode electrochemical sensing system, Ag/AgCl paste was lined over the right side of the silver ink-coated array and assigned as the reference electrode. Similarly, the central carbon ink coated square shape array was further modified with carbon dots to construct a micro-nano hierarchical structure on the surface of the working electrode microneedle array for improved sensing performance. The left side L-shaped carbon-coated array was assigned as the counter electrode. To create good electrical connections, a conductive silver epoxy was lined over the connecting legs. In the next step, the microneedle portion was covered with a 3D-printed thin cover to avoid any unwanted electrical contacts other than at the tip area. Afterward, the as-developed fully assembled conductive microneedle array-based sensing platform was used for the electrochemical sensing of chlorpromazine *via* a wireless potentiostat and the collected differential pulse voltammetry response was sent to the personalized computer for further data analysis.

3.2 Fabrication and characterization of the conductive microneedle array

Computer-aided design software and modern 3D printers have offered ease in manufacturing and modifying the dimensions, configurations, and structure of microneedles, enabling us to prepare the customized microneedle array for this study. 3D printing has evolved as an economical and scalable fabrication technique for manufacturing various healthcare devices. An ultra-sharp microneedle array structure having 67 conical shape needles with a height of 1200 μm and base diameter of 350 μm for the development of a microneedle-based transdermal sensing platform was designed in SolidWorks 2016 software and printed using the BMF S130 3D-printer. Because the transdermal biosensing technique needs a material that can easily penetrate the stratum layer of the skin without any damage to the surrounding tissues, a yellow color photoreactive biocompatible resin BIO having appropriate hardness and Young's modulus values was used for the 3D printing of the microneedle array. Fig. 2 shows realistic photographs of step-by-step manufacturing of the proposed microneedle array-based sensing platform. The as-printed microneedle array shown in Fig. 2a was modified with different inks using a Dimatix inkjet printer; a macroscopic image of the inkjet-printed microneedle array is shown in Fig. 2b. To make an electroactive three-electrode system on the tips of the

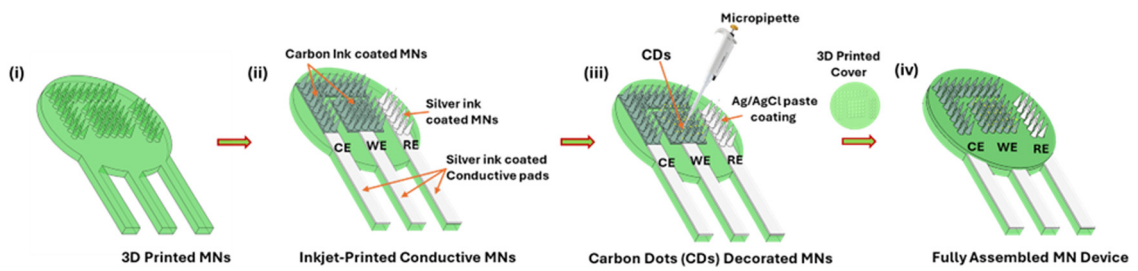

Fig. 1 Schematic diagram of stepwise fabrication process for the three-electrode system on the tips of microneedle array using 3D printing and inkjet printing techniques: (i) 3D-printed microneedle array, (ii) inkjet-printed conductive microneedle array, (iii) carbon dots-decorated working electrode microneedles and Ag/AgCl paste coating on reference electrode microneedles, and (iv) fully assembled three-electrode system-based microneedle device.

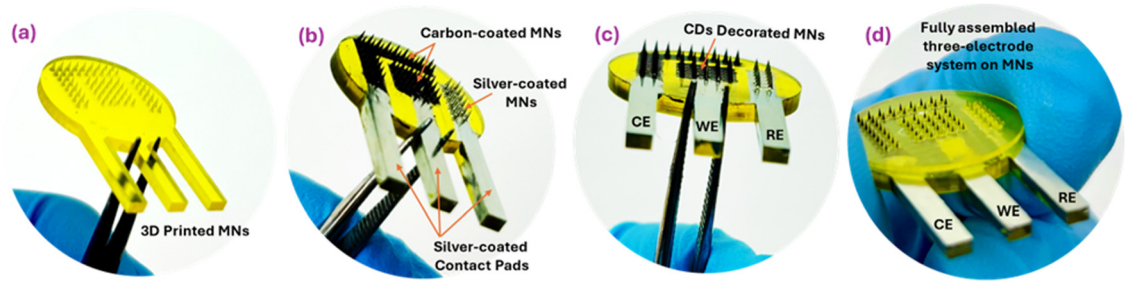

Fig. 2 Illustration of 3D-printed ultra-sharp microneedle array. Realistic macroscopic images of (a) as-printed (yellow) microneedle array, (b) inkjet-printed carbon-coated conductive (black) microneedle array and sliver ink-coated contact pads, (c) carbon dots decorated working electrode microneedles and Ag/AgCl paste coated reference electrode microneedles, and (d) fully assembled three-electrode system on the tips of microneedles covered by a 3D printed cover to avoid any unwanted electrical contact other than at the tip area.

microneedle array, the carbon ink-coated central 5 × 5 array was decorated with carbon dots, followed by deposition of the protective biopolymeric layer to avoid potential leaching from the needle surface; this structure served as the working electrode (Fig. 2c). Similarly, the right side 2 × 6 array was coated with Ag/AgCl paste and assigned as the reference electrode. The remaining L-shaped carbon-coated array was assigned as the counter electrode. Fig. 2d demonstrates the macroscopic image of a 3D printed cover encompassing a fully assembled and ready-to-use microneedle array-based sensing platform. To assess the three-dimensional topographical microscale features of the tip and ensure the successful fabrication of a sharp microneedle array, scanning electron microscope (SEM) images of the as-printed, silver and carbon ink-coated, and Nafion layer deposited microneedle array were collected and are shown in Fig. 3. Fig. 3a and b show the SEM image of a 3D-printed solid microneedle array and the magnified SEM image of a single microneedle, respectively. It can be observed that the space between the microneedles was consistent; the build layers of the microneedle design were uniform and reproducible. The 3D printer, which uses projection micro stereolithography (PμSL) technology, facilitated the consistent production of microneedle arrays with outstanding microscale features, leading to the fabrication of ultra-sharp needle tips required for skin penetration. Thus, printing using a BMF 3D printer with economic and biocompatible resin renders an attractive method for microneedle fabrication. Fig. 3c and d show an SEM image of a silver ink-printed microneedle array and the magnified SEM image of a single microneedle, respectively. It can be noted that the silver ink was deposited consistently and uniformly on each microneedle without any bulky coating features, which are commonly observed in coatings made with the conventional dip coating technique. Similarly, the uniform coating of carbon ink on the microneedles is shown in Fig. 3e (microneedle array) and Fig. 3f (magnified SEM image of a single microneedle from the array). Further, the cloudiness and blurriness reflected in Fig. 3g (microneedle array) and Fig. 3h (magnified SEM image of a single microneedle from the array) indicate the successful and uniform deposition of Nafion biopolymeric layer on the microneedle array surface. These results reveal that the inkjet

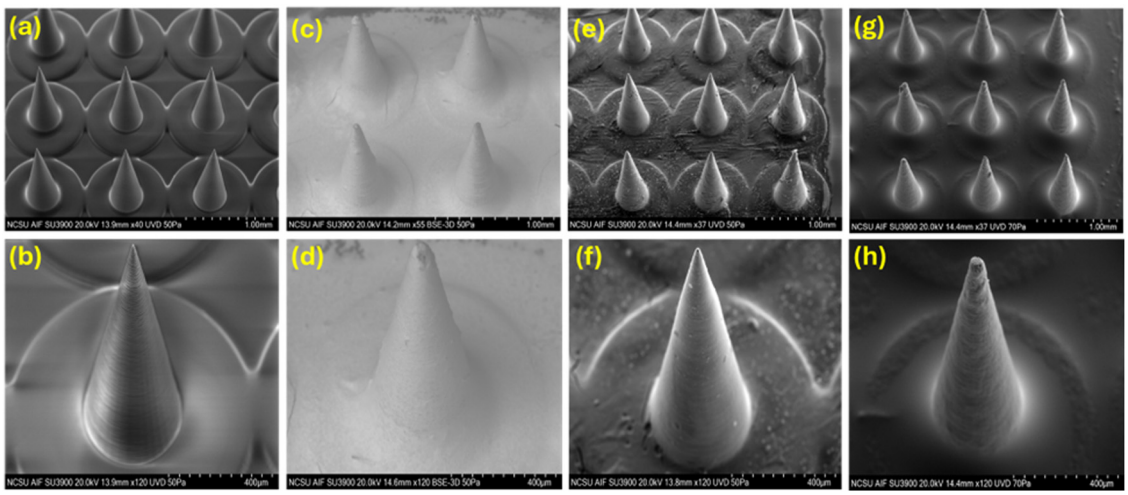

Fig. 3 Illustration of microscale details of as-printed and surface-modified microneedle array through scanning electron microscope (SEM) images. SEM images of (a) uncoated 3D printed microneedle array, and (b) single microneedle surface from the array. SEM images of (c) silver ink-coated microneedle array, and (d) single microneedle surface from the array. SEM images of (e) carbon-coated microneedle array, and (f) single microneedle surface from the array. SEM images of (g) Nafion biopolymeric layer deposited microneedle array, and (h) single microneedle surface from the array.

printing facilitated the uniform deposition of different inks on the microneedle surface with high accuracy. The skin penetration capability of the developed microneedle array-based sensing platform also plays an essential role in assessing the feasibility of the wearable device. A human skin mimicking porcine skin patch was used to examine the skin penetration characteristics of the microneedle array. Fig. 4a–d contain macroscopic and microscopic pictures of porcine skin before and after puncture with a microneedle array. Fig. 4a shows the macroscopic image of clean and sanitized pig skin that was obtained from a regional provider. Fig. 4b shows the optical image of sanitized skin patch before penetration; Fig. 4c and d show the optical images of different portions of the skin patch after penetration by a microneedle array. These images demonstrate that the developed microneedle array penetrated the skin in a topographically-limited manner without injury to the neighboring portion of skin; this result confirms the array can be used for the development of wearable sensing devices.

3.3 Electrochemical activity, chlorpromazine sensing, and selectivity assay

Prior to using the fully assembled microneedle-based sensing platform for the detection of chlorpromazine, the electrochemical activity and stability of the three-electrode system based on the microneedles were investigated. Here, the cyclic voltammetry technique was used to understand the redox behavior of the as-developed three-electrode system on the microneedle array in a freshly prepared 3 mM ferricyanide solution at a constant scan rate of 50 mV s^{-1}. The obtained green color cyclic voltammetry spectra shown in Fig. 4e exhibited a desirable reversible redox behavior, demonstrating the effective electrochemical charge transfer activity of the printed conductive microneedle electrode. The cyclic voltammetry spectra of carbon dots modified working electrode were recorded to understand the effect of the carbon dots on the electroanalytical performance of carbon-coated microneedle-based working electrode. The obtained orange color cyclic voltammetry spectra shown in Fig. 4e indicate a significant difference in the peak current value after the deposition of carbon dots, suggesting that micro-nano hierarchical structure facilitated by the carbon dots on the microneedle surface has a notable effect on electron transfer dynamics at the electrode interface. Further, the consistency and stability of the as-developed three-electrode system on the microneedle array can affect the real-time application and performance of the device; thus, the electrochemical stability of the carbon dots decorated carbon coated microneedle-based working electrode was examined by collecting four cyclic voltammetry response scans. It was noted (Fig. 4f) that the cyclic voltammetry response of all four scans was well overlapped, suggesting the same oxidation and reduction peak for multiple scans; this result confirms the desirable stability and electrochemical consistency of the developed microneedle-based sensing platform. After understanding the electrochemical activity and stability of the developed microneedle-based three-electrode sensing system, the electrochemical analytical performance of carbon dots-modified microneedle-based working electrode

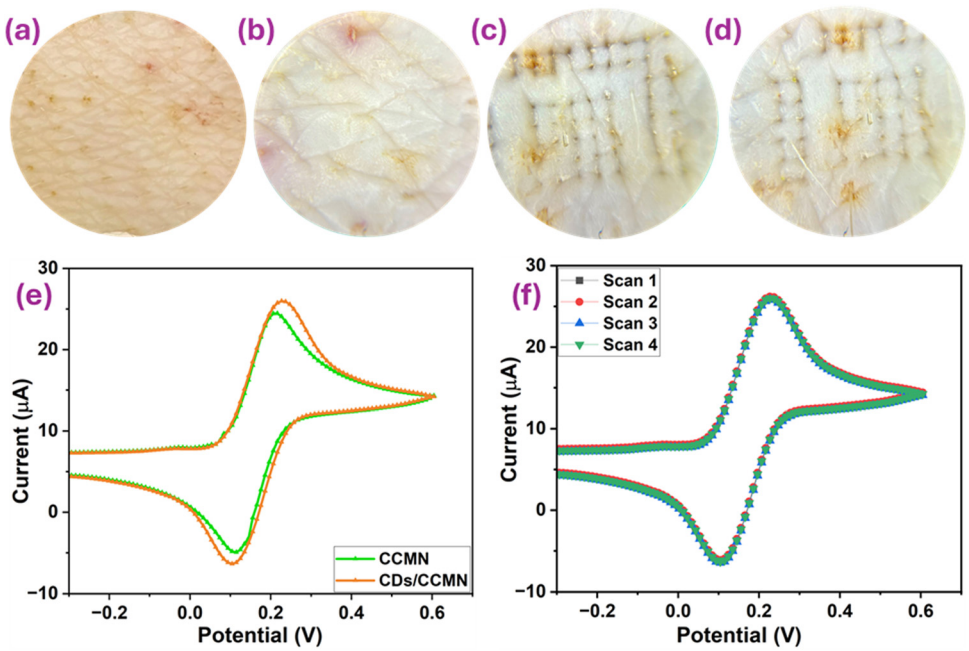

Fig. 4 Illustration of skin penetration, electrochemical characteristics, and electrode stability of developed microneedle array-based sensing platform. Illustration of (a) realistic photo and (b) optical microscopic image of clean and sanitized pig skin before skin penetration. Optical microscopic image of microneedle arrays punctured pig skin (c) showing the insertion of working and counter electrode, and (d) showing the insertion of the reference electrode and working electrode. (e) Cyclic voltammetry response of the as-developed three-electrode system on the microneedle array before and after carbon dots deposition, and (f) multiple scans of carbon dots deposited carbon coated microneedle array in freshly prepared 3 mM ferricyanide solution at a constant scan rate of 50 mV s^{-1}.

towards varying concentrations (5–120 μM) of chlorpromazine was examined *via* the differential pulse voltammetry method. The collected differential pulse voltammetry spectra for increasing concentrations of chlorpromazine are displayed in Fig. 5a. It was noticed from the differential pulse voltammetry spectra that the developed microneedle-based sensing system exhibited a gradual increase in the peak current with increasing concentration of chlorpromazine in the range from 5 to 120 μM. Subsequently, the respective peak current values were plotted corresponding to the increasing concentration of chlorpromazine; a linear correlation between the peak current and chlorpromazine concentration was noted, with an R^2 value of 0.982 (as demonstrated in Fig. 5b). Further, the lower detection limit was determined through the equation $3s/M$, where M represents the slope and s denotes the standard error; it was found to be as low as 0.09 μM. Further, Fig. 5c demonstrates the possible electrochemical reaction mechanism of chlorpromazine occurring on the tip of microneedles. Although the electrochemical analytical performance results of the developed microneedle-based sensing platform confirmed the sensing potential of the probe, the selectivity for chlorpromazine is also an important parameter to assess the efficacy of an electrochemical sensing system. As such, the selectivity assay was performed by evaluating the change in current value in the presence of potential interferents, including acetaminophen, ascorbic acid, dopamine, caffeine, and uric acid; the differential pulse voltammetry response for all interferents was obtained while adding a given amount (50 μM) of interfering compound and keeping all other experimental factors constant. The obtained spectra demonstrated some changes in the peak current value for all of the interfering compounds, as shown in Fig. 5d. All potential interfering compounds used in the selectivity assay can indicate an oxidation reaction on the electrode surface; we observed some peak current for all interfering compounds. However, the value of the peak potential was different for the interferants, as shown in Fig. S2 (ESI†). Even though the interferants exhibited some current response, the peak current value for chlorpromazine was significantly higher than the peak current value of other interfering compounds. Consequently, these analytical study results confirm that the proposed microneedle-based sensing probe is highly sensitive and selective for chlorpromazine.

3.4 Real-time application in a skin-mimicking models and long-term stability

After understanding the desired sensing capabilities of the developed protective biopolymeric layer deposited carbon dots-decorated carbon-coated microneedle-based sensing platform, the real-time application potential and efficiency of the microneedle-based sensor were further explored by detecting chlorpromazine through a skin-mimicking parafilm layer in artificial interstitial fluid and phantom gel model *via* the differential pulse voltammetry technique. Fig. 6a shows the realistic photograph of the experimental setup used for the real-time application study. In this approach, a skin-mimicking parafilm tape-wrapped Petri plate was filled with artificial interstitial fluid and spiked with six different concentrations of chlorpromazine; the corresponding differential pulse voltammetry spectra were recorded between a potential window ranging from −0.1 to 0.5 V at a potential step of 0.01 V. The collected differential pulse voltammetry results (shown in Fig. 6b) reveal a noticeable change in the peak current value with the addition of chlorpromazine. Further, for the quantitative estimation, a calibration curve (Fig. 6c) was plotted between these peak current values and the spiked chlorpromazine concentration, which showed the good linearity and desirable sensitivity of fully assembled microneedle-based sensing platform (Fig. 6c, inset) towards chlorpromazine. Further, the real time sensing capabilities of the microneedle sensor

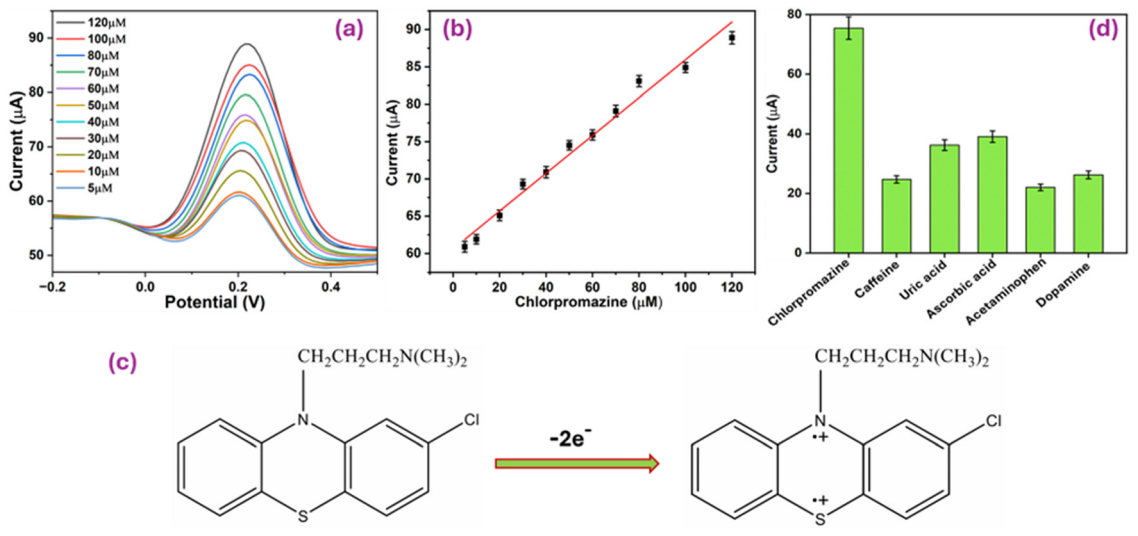

Fig. 5 Illustration of electrochemical reaction mechanism, sensing, and selectivity potential of developed microneedle array-based sensor. (a) Differential pulse voltammetry response of the carbon dots-modified microneedle array electrode for increasing concentrations of chlorpromazine, (b) corresponding calibration plot between the peak values and chlorpromazine concentration, (c) electrochemical reaction mechanism of chlorpromazine on the surface of microneedle array, and (d) selectivity assay of developed sensing platform in the presence of potential interfering compounds.

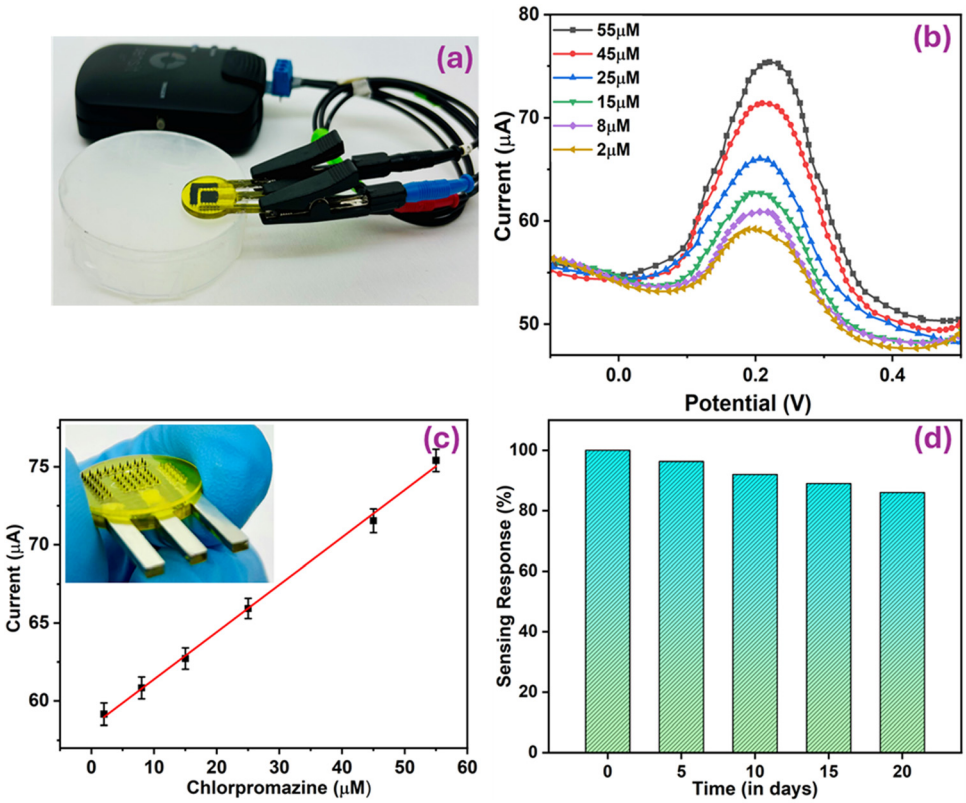

Fig. 6 Proof-of-concept demonstration of fully assembled microneedle sensor. (a) Illustration of a realistic photograph of experimental setup that was utilized in the proof-of-concept demonstration for the detection of chlorpromazine through a skin-mimicking parafilm layer in artificial interstitial fluid, (b) differential pulse voltammetry response of fully assembled microneedle sensor towards increasing concentrations of chlorpromazine, (c) corresponding calibration plot between the peak values and chlorpromazine concentration (inset: Real photo of fully assembled microneedle sensor), and (d) long-term stability of the developed microneedle array-based sensor.

were assessed by executing chlorpromazine detection in a phantom gel model. It was studied from Fig. S1 (ESI†) that the developed sensing platform sensor demonstrated a obvious change in the current value for all concentrations of chlorpromazine infused in the phantom gel and exhibited a good linearity in the calibration plot (Fig. S1b, ESI†), suggesting the on-body chlorpromazine detection potential of the sensor. Next, the long-term stability of the fully assembled microneedle sensor was evaluated by assessing the variation in the sensing performance at five-day periods until twenty days. The obtained results, shown in the bar graph (Fig. 6d), indicated that the fabricated microneedle sensor retained 86% of the analytical performance despite 20 days of storage. These results confirm that the 3D-printed conducting microneedle array-based three-electrode system developed in this study can readily detect the micromolar levels of chlorpromazine under the skin with high sensitivity and long-term stability.

4. Conclusions

We demonstrated a scalable manufacturing process for the development of an electrochemical point-of-care device containing a 3D-printed conducting microneedle array for the minimally invasive sensing of chlorpromazine. The microneedle array exhibited high sensitivity, a low detection limit, and desirable selectivity towards chlorpromazine, along with good linearity in artificial interstitial fluid during a study that involved penetration of a skin-mimicking parafilm layer. The proposed sensor-on-microneedle technology was developed using two additive manufacturing procedures (3D printing and inkjet printing) for painless skin penetration, straightforward assembly, high reproducibility, low-cost manufacturing, and scalable medical device production. The analytical performance results and ease of fabrication of the developed microneedle sensors indicate that such a novel approach can be used to create different low-cost and single-use electrochemical biosensors for biomolecule detection in interstitial fluid. Future efforts will include the integration of a multiplex sensing system onto the conducting microneedle electrode array for the simultaneous detection of multiple biomarkers, along with a fully integrated wearable patch with battery and wireless electronics components.

Data availability

The data collected throughout the course of the study is presented and detailed within the main sections of the manuscript.

Conflicts of interest

There are no personal or financial conflicts to declare for this study.

Acknowledgements

Authors acknowledge the support from National Science Foundation Award Number 2029974. This work was performed in part at the Analytical Instrumentation Facility (AIF) at North Carolina State University, which is supported by the State of North Carolina and the National Science Foundation (award number ECCS-2025064). The AIF is a member of the North Carolina Research Triangle Nanotechnology Network (RTNN), a site in the National Nanotechnology Coordinated Infrastructure (NNCI).

References

1 Y. Kyotani, J. Zhao, K. Nakahira and M. Yoshizumi, *Sci. Rep.*, 2023, **13**, 18459.
2 T. A. Ban, *Neuropsychiatr. Dis. Treat.*, 2007, **3**, 495.
3 K. Dudley, X. Liu and S. De Haan, Chlorpromazine dose for people with schizophrenia, *Cochrane Database Syst. Rev.*, 2017, **4**, 1–7.
4 P. Kaleeswarran, B. Sriram, S. F. Wang, J. N. Baby, A. Arumugam, A. L. Bilgrami, S. A. Hashsham, F. Abdullah Sayegh and C. J. Liu, *Microchem. J.*, 2021, **163**, 105886.
5 S. W. Woods, *J. Clin. Psychiatry*, 2003, **64**(6), 663–667.
6 N. Tavakkoli, N. Soltani, H. Salavati and M. Talakoub, *J. Taiwan Inst. Chem. Eng.*, 2018, **83**, 50–58.
7 H. B. Wang, H. D. Zhang, L. L. Xu, T. Gan, K. J. Huang and Y. M. Liu, *J. Solid State Electrochem.*, 2014, **18**, 2435–2442.
8 T. J. Mellinger and C. E. Keeler, *Anal. Chem.*, 1964, **36**, 1840–1847.
9 M. Conneely, D. Roe, I. Hasson-Ohayon, G. H. M. Pijnenborg, L. van der Meer and H. Speyer, *Community Ment. Health J.*, 2024, 1–6.
10 I. J. D. Priscillal and S. F. Wang, *Microchem. J.*, 2023, **187**, 108396.
11 M. Chatterjee, P. Nath, S. Kadian, A. Kumar, V. Kumar, P. Roy, G. Manik and S. Satapathi, *Sci. Rep.*, 2022, **12**, 9061.
12 S. Kadian, N. Chaulagain, N. N. Joshi, K. M. Alam, K. Cui, K. Shankar, G. Manik and R. J. Narayan, *Nanotechnology*, 2023, **34**, 30LT01.
13 S. Kadian, S. Gopalakrishnan, V. Selvamani, S. Khan, T. Meyer, R. Thomas, M. M. Rana, P. P. Irazoqui, M. Verma and R. Rahimi, *IEEE Trans. Biomed. Eng.*, 2023, **1**, 1565–1576.
14 S. Kadian, N. Chaulagain, H. Rajashekhar, D. Vrushabendrakumar, G. Manik and K. Shankar, *Proc. IEEE Sens.*, 2021, 1–4.
15 S. Ren, J. Zeng, Z. Zheng and H. Shi, Perspective and application of modified electrode material technology in electrochemical voltammetric sensors for analysis and detection of illicit drugs, *Sens. Actuators, A*, 2021, **329**, 112821.
16 M. Razlansari, F. Ulucan-Karnak, M. Kahrizi, S. Mirinejad, S. Sargazi, S. Mishra, A. Rahdar and A. M. Díez-Pascual, Nanobiosensors for detection of opioids: A review of latest advancements, *Eur. J. Pharm. Biopharm.*, 2022, **179**, 79–94.
17 D. Beduk, T. Beduk, J. I. de Oliveira Filho, A. Ait Lahcen, E. Aldemir, E. Guler Celik, K. N. Salama and S. Timur, *ACS Appl. Mater. Interfaces*, 2023, **15**(31), 37247–37258.
18 S. Kadian and G. Manik, *Luminescence*, 2020, **35**, 763–772.
19 S. Kadian, P. Kumari, S. Shukla and R. Narayan, *Talanta Open*, 2023, **8**, 100267.
20 S. Kadian, G. Manik, A. Kalkal, M. Singh and R. P. Chauhan, *Nanotechnology*, 2019, **30**, 435704.
21 A. Krishnakumar, R. K. Mishra, S. Kadian, A. Zareei, U. H. Rivera and R. Rahimi, *Anal. Chim. Acta*, 2022, **1229**, 340332.
22 T. A. Tabish, Y. Zhu, S. Shukla, S. Kadian, G. S. Sangha, C. A. Lygate and R. J. Narayan, *Appl. Phys. Rev.*, 2023, **10**, 041310.
23 S. Kadian, B. D. Arya, S. Kumar, S. N. Sharma, R. P. Chauhan, A. Srivastava, P. Chandra and S. P. Singh, *Electroanalysis*, 2018, **30**, 2793–2802.
24 Z. Lu, K. Wei, H. Ma, Q. Xiong, Y. Li, M. Sun, X. Wang, Y. Wang, C. Wu, G. Su, Y. Bai, R. Deng, J. Ye, C. Zhou and H. Rao, *Sep. Purif. Technol.*, 2023, **327**, 124858.
25 Q. Han, T. Zhang, M. Wang, F. Yan and J. Liu, *Molecules*, 2022, **27**, 8200.
26 V. N. Palakollu, R. Karpoormath, L. Wang, J. N. Tang and C. Liu, *Nanomaterials*, 2020, **10**, 1513.
27 K. Y. Goud, C. Moonla, R. K. Mishra, C. Yu, R. Narayan, I. Litvan and J. Wang, *ACS Sens.*, 2019, **4**, 2196–2204.
28 R. K. Mishra, K. Y. Goud, Z. Li, C. Moonla, M. A. Mohamed, F. Tehrani, H. Teymourian and J. Wang, *J. Am. Chem. Soc.*, 2020, **142**, 5991–5995.
29 U. Heredia-Rivera, S. Gopalakrishnan, S. Kadian, S. Nejati, V. Kasi and R. Rahimi, *J. Mater. Chem. C*, 2022, **10**(26), 9813–9822.
30 A. Krishnakumar, S. Kadian, U. Heredia Rivera, S. Chittiboyina, S. A. Lelièvre and R. Rahimi, *ACS Biomater. Sci. Eng.*, 2022, **3**, 1620–1628.
31 U. Heredia-Rivera, V. Kasi, A. Krishnakumar, S. Kadian, A. K. Barui, Z. He, H. Wang, L. Stanciu and R. Rahimi, *ACS Appl. Mater. Interfaces*, 2023, **15**, 17078.
32 S. Kadian, P. Kumari, S. S. Sahoo, S. Shukla and R. J. Narayan, *Microchem. J.*, 2024, **200**, 110350.
33 Z. Li, S. Kadian, R. K. Mishra, T. Huang, C. Zhou, S. Liu, Z. Wang, R. Narayan and Z. Zhu, *J. Mater. Chem. B*, 2023, **26**, 6075–6081.
34 S. Kadian, S. S. Sahoo, P. Kumari, S. Shukla and R. J. Narayan, *Microchim. Acta*, 2024, **191**, 672.
35 T. Bedir, S. Kadian, S. Shukla, O. Gunduz and R. Narayan, *Expert Opin. Drug Delivery*, 2024, **21**, 1053.
36 S. Kadian, P. Kumari, S. S. Sahoo, S. Shukla and R. J. Narayan, *Microchem. J.*, 2024, **200**, 110350.
37 S. A. Machekposhti, S. Kadian, L. Vanderwal, S. Stafslien and R. J. Narayan, *MedComm*, 2023, **4**, e321.
38 S. Shukla, N. N. Joshi, S. Kadian and R. J. Narayan, *ACS Appl. Bio. Mater.*, 2024, **7**, 5382.
39 S. Shukla, S. Kadian and R. J. Narayan, *J. Solid State Electrochem.*, 2024, 1–22.

40 S. Kadian, S. Shukla and R. J. Narayan, *Appl. Phys. Rev.*, 2023, **10**, 041304.
41 S. Kadian, S. S. Sahoo, P. Kumari and R. J. Narayan, *Electrochim. Acta*, 2024, **475**, 143664.
42 S. Shukla, J. Jakowski, S. Kadian and R. J. Narayan, *Comput. Struct. Biotechnol. J.*, 2023, **21**, 4149.
43 J. Kim, I. Jeerapan, J. R. Sempionatto, A. Barfidokht, R. K. Mishra, A. S. Campbell, L. J. Hubble and J. Wang, *Acc. Chem. Res.*, 2018, **51**, 2820–2828.
44 S. Shukla, S. A. Machekposhti, N. Joshi, P. Joshi and R. J. Narayan, *Small Sci.*, 2023, **3**, 2200087.
45 S. Kadian, G. Manik, N. Das and P. Roy, *Microchim. Acta*, 2020, **187**, 1–10.
46 S. Kadian and G. Manik, *Food Chem.*, 2020, **317**, 126457.
47 S. Kadian, A. Kalkal, V. Jain, S. Shukla and R. J. Narayan, *MRS Commun.*, 2023, **13**(5), 885–891.
48 S. Kadian, N. K. Tailor, N. Chaulagain, K. Shankar, S. Satapathi and G. Manik, *J. Mater. Sci.:Mater. Electron.*, 2021, **32**, 17406.
49 N. Chaulagain, K. M. Alam, S. Kadian, N. Kumar, J. Garcia, G. Manik and K. Shankar, *ACS Appl. Mater. Interfaces*, 2022, **14**, 24309.
50 J. J. García-Guzmán, C. Pérez-Ràfols, M. Cuartero and G. A. Crespo, Microneedle based electrochemical (Bio)Sensing: Towards decentralized and continuous health status monitoring, *TrAC, Trends Anal. Chem.*, 2021, **135**, 116148.